JOURNAL OF GEOPHYSICAL RESEARCH, VOL. 116, D08103, doi:10.1029/2010JD015157, 2011

Evaluation of mesoscale convective systems in South America using multiple satellite products and an object-based approach

E. M. C. Demaria,[1] D. A. Rodriguez,[2] E. E. Ebert,[3] P. Salio,[4] F. Su,[5] and J. B. Valdes[1]

Received 8 October 2010; revised 25 January 2011; accepted 28 January 2011; published 19 April 2011.

[1] In this study, an object-based verification method was used to reveal the existence of systematic errors in three satellite precipitation products: Tropical Rainfall Measurement Mission (TRMM), Climate Prediction Center Morphing Technique (CMORPH), and Precipitation Estimation from Remotely Sensed Information Using Artificial Neural Networks (PERSIANN). Mesoscale convective systems (MCSs) for the austral summer 2002–2003 in the La Plata river basin, southeastern South America, were analyzed with the Contiguous Rain Area (CRA) method. Errors in storms intensity, volume, and spatial location were evaluated. A macroscale hydrological model was used to assess the impact of spatially shifted precipitation on streamflows simulations. PERSIANN underestimated the observed average rainfall rate and maximum rainfall consistent with the detection of storm areas systematically larger than observed. CMORPH overestimated the average rainfall rate while the maximum rainfall was slightly underestimated. TRMM average rainfall rate and rainfall volume correlated extremely well with ground observations whereas the maximum rainfall was systematically overestimated suggesting deficiencies in the bias correction procedure to filter noisy measurements. The preferential direction of error displacement in satellite-estimated MCSs was in the east-west direction for CMORPH and TRMM. Discrepancies in the fine structure of the storms dominated the error decomposition of all satellite products. Errors in the spatial location of the systems influenced the magnitude of simulated peaks but did not have a significant impact on the timing indicating that the system's response to precipitation was mitigating the effect of the errors.

Citation: Demaria, E. M. C., D. A. Rodriguez, E. E. Ebert, P. Salio, F. Su, and J. B. Valdes (2011), Evaluation of mesoscale convective systems in South America using multiple satellite products and an object-based approach, *J. Geophys. Res.*, *116*, D08103, doi:10.1029/2010JD015157.

1. Introduction

[2] Estimates of precipitation in fine spatial and temporal resolutions are required for many hydrological applications. Until recently, satellite precipitation estimates were only available at coarse resolutions not suitable for the implementation of hydrological models in large basins at daily or subdaily time scales. In the last decade, remotely sensed rainfall has became increasingly accessible to a wider population outside the atmospheric community and several products are available at temporal and spatial scales that are potentially useful for flood monitoring, flash flood, landslide forecasting, and for water resources management, to name a few. Not only available satellite estimates of precipitation allow the accurate representation of the hydrological cycle in a basin, in underdeveloped regions of the world they constitute the only existing source of meteorological information. However, satellite estimates of precipitation are prone to errors and need to be verified using ground measurements [*Ebert et al.*, 2007; *Xie and Arkin*, 1995]. There exists a substantial body of literature assessing the agreement between satellite products and ground based measurements at different temporal and spatial scales in data-rich regions of the world [e.g., *Bell and Kundu*, 2000; *Astin*, 1997; *Huffman*, 1997; *Salby and Callaghan*, 1997]. However, in South America, few studies have assessed the validity of satellite products at scales of utility for hydrological applications. *de Goncalves et al.* [2006] investigated the reliability of model and satellite estimated 24 h precipitation fields using rain gauge measurements. They found that satellite estimates of rainfall show difficulties representing the area with precipitation and the

[1]Department of Hydrology and Water Resources and SAHRA, University of Arizona, Tucson, Arizona, USA.
[2]Earth System Science Center, National Institute for Space Research, Cachoeira Paulista, Brazil.
[3]Centre for Australian Weather and Climate Research, Melbourne, Victoria, Australia.
[4]Centro de Investigaciones del Mar y la Atmósfera, CONICET/UBA, and Departamento de Ciencias de la Atmósfera y los Océanos, Universidad de Buenos Aires, Buenos Aires, Argentina.
[5]Department of Civil and Environmental Engineering, University of Washington, Seattle, Washington, USA.

0148-0227/11/2010JD015157

magnitude of the rainfall event. *Su et al.* [2008] used a hydrological model to assess the effectiveness of multi-satellite precipitation products for hydrologic predictions. Their results showed a good agreement between satellite and rain gauge driven simulated flows indicating that multi-satellite products can efficiently reproduce the seasonal and interannual variability of flows in the La Plata river basin. Recently, the land-surface community has started to combine remotely sensed information with rain gauge measurements to create high-resolution atmospheric data sets through assimilation techniques [*de Goncalves et al.*, 2009; *Vila et al.*, 2009].

[3] All previous studies in South America have measured the accuracy of rainfall amount or rainfall intensity averaged over an area using verification statistics such as bias, root mean square error (RMSE), correlation coefficient and/or categorical verification statistic, i.e., contingency tables, bias score, probability of detention and false alarm ratios [*Stanski et al.*, 1989]. Even though these types of statistics provide valuable insight on how closely two fields correspond in time, the hydrology community requires more specific information about expected errors on rain location, mean and maximum intensities for specific storm types since the spatial and temporal distribution of rainfall highly impact streamflow properties. Storm characteristics, i.e., amount, intensity and duration of the event, velocity and direction of the storm, and genesis of the storm, are some of the factors affecting streamflow generation in a basin. Variations of these factors in space and/or time affect the magnitude and the timing of peak flows [*Nunes et al.*, 2006; *Singh*, 2002a, 2002b, 1997].

[4] An alternative approach to continuous and categorical verification techniques is the evaluation of rain entities using an object-based approach, which allows the verification of the bulk properties of the satellite estimated rain field against the bulk properties of the reference field or observations [*Gilleland et al.*, 2009]. *Ebert and McBride* [2000] developed the Contiguous Rain Area (CRA) method in which the total mean squared error of a rainfall event, i.e., storm, is determined by matching the pattern of the estimated and observed fields in a cell-by-cell analysis. The location error is determined by horizontally shifting the precipitation estimates over the observations until a best fit is found minimizing or maximizing a user-defined objective function.

[5] The southeastern part of South America (SESA) is susceptible to some of the most intense storm events on Earth whose heavy precipitation generates numerous cases of severe weather and flooding [*Zipser et al.*, 2006; *Silva Dias*, 1999]. During the warm season the precipitation in SESA is modulated by the presence of mesoscale processes associated with the activity of mesoscale convective systems (MCSs). Their typical organizational structure involves a deep convective part that can produce high rates of rainfall in a brief period of time, and a stratiform part with moderate precipitation but extended durations [*Doswell et al.*, 1996]. Due to their spatial extension and high intensities MCSs are also capable of generating flash flood events [*Teixeira and Satyamurty*, 2007]. MCSs comprise mesoscale convective complexes, squall lines, and precipitation bands [*Hirschboeck et al.*, 2000].

[6] Studies indicate that in SESA precipitation from mesoscale convective complexes alone contribute with up to 60% of the total rainfall [*Durkee et al.*, 2009; *Durkee and Mote*, 2009]. Using TRMM satellite estimates *Mota* [2003] estimated that MCSs produce approximately 80% of the total precipitation in SESA. However, despite substantial economic losses, large number of people being displaced, and flood-related death toll, there are no standardized procedures to document and mitigate the impacts of severe storms in the region [*Nascimento and Doswell*, 2006]. In addition to the lack of institutional efforts to anticipate the occurrence and minimize the impacts of intense rainfall events in SESA, it is the need for an adequate ground network of radars and rain gauges that enable the study and monitoring of such destructive events. Quite clearly, satellite-based precipitation estimates are of greatest interest in this part of the globe where observation networks are sparse and local inhabitants are most susceptible to hydrologic extremes.

[7] The overriding goal of this study is to use the CRA method to reveal the existence of systematic errors in remotely sensed precipitation products in SESA during the warm season. We argue that a significant improvement in flash flood forecasting and warning systems can be achieved if the existence of systematic errors in satellite-estimated storms can be quantified. A secondary goal is to investigate how errors in the location of MCSs propagate through the hydrological cycle and have an impact on the characteristics of streamflows in a basin.

[8] The paper is organized as follows: section 2 presents a description of the basin and the data sets used in the study. The methodological approach is introduced in section 3. Results of CRA analysis and the case study are outlined in sections 4 and 5, respectively. Finally, main conclusions of the study are presented in section 6.

2. Study Area and Data Sets

[9] The La Plata river basin (LPB) is the second largest river system in South America after the Amazon River Basin. It covers approximately 3.2×10^6 km^2 and is located between 14°S and 38°S latitude and between 67°W and 43°W longitude (Figure 1). The basin is shared by five countries: Brazil occupies approximately 46% of its surface, Argentina 30%, Paraguay 13%, Bolivia 7% and Uruguay 4%. The mean annual precipitation in the LPB shows a maximum of 1,500 mm in the central eastern portion of the basin with lesser amounts to the south and west [*Berbery and Barros*, 2002]. The annual cycle of precipitation presents two distinctive precipitation maxima: one along the northern boundary during the austral summer and the second one in the southern region of the basin during spring and fall [*Rodriguez and Cavalcanti*, 2006]. The atmospheric water cycle of the LPB is significantly influenced by mesoscale variability associated with the existence of a low-level circulation located east of the Andes [*Nogués-Paegle et al.*, 2002].

[10] Three satellite-based precipitation products were selected for the study. The first two data sets use an adjustment technique to correct Infrared (IR) cloud top temperatures using an independent data set such as precipitation radar and/or microwave radiometer measurements;

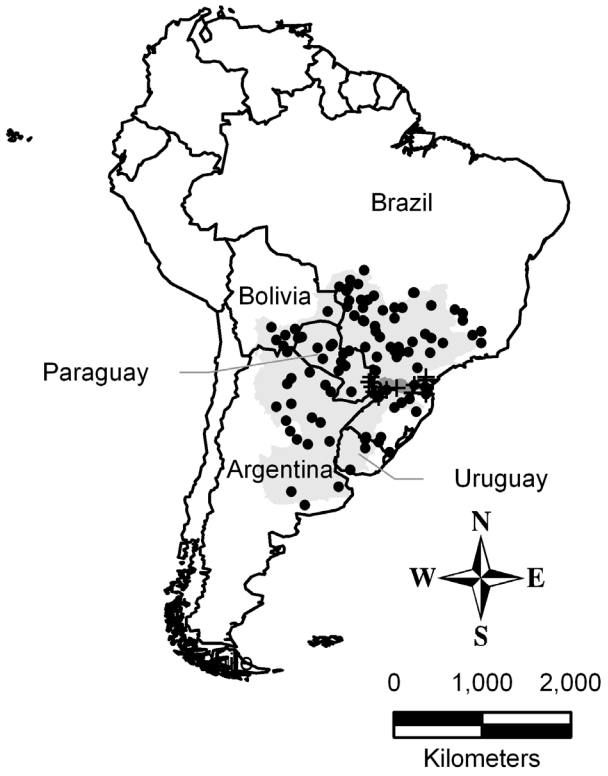

Figure 1. Geographical location of the La Plata River Basin. The light gray shaded area represents the geographical extension of the La Plata basin and the dark gray area corresponds to the Iguazu basin. The dots represent the latitude and longitude of the centroid of each MCS identified during the summer 2002–2003, and the crosses represent the systems identified in the Iguazu basin during the period 2001–2003.

the third data set exclusively relies on microwave observations that are spatially propagated using high temporal resolution IR values from geostationary satellites [*Kidd et al.*, 2009]. Microwave data have a strong physical relationship with the hydrometeors that generate surface precipitation but their time-space coverage is quite sparse since the microwave instruments are carried on low-orbit satellites. Infrared estimates, on the other hand, have excellent space-time coverage but cloud top temperature does not always correlate well with rainfall.

[11] The Tropical Rainfall Measuring Mission 3B42v6 research version (TRMM) relies primarily on passive microwave precipitation estimates (PMW) from the Special Sensor Microwave Imager (SSM/I), the TRMM Microwave Imager (TMI), the Advanced Microwave Sounding Unit (AMSU), and the Advanced Microwave Scanning Radiometer for Earth Observing System (AMSR-E). The PMW data are first calibrated using the combined TMI and TRMM precipitation radar product (PR) and then used to calibrate geosynchronous IR inputs. Monthly surface rainfall observations are used to bias-correct the multisatellite product [*Huffman et al.*, 2007]. The TRMM data set covers the latitude band 50°S to 50°N from 1998 to the present and is available at 3-hourly temporal resolution in a 0.25-degree box.

[12] The Precipitation Estimation from Remotely Sensed Information Using Artificial Neural Networks (PERSIANN) data set is available at the same spatial resolution of TRMM but every 6 h. PERSIANN uses an artificial neural network to process geostationary longwave IR imagery to generate global rainfall. The neural network parameters are regularly updated using TMI, SSM/I, and AMSU estimates [*Hsu et al.*, 1997]. This rainfall product covers the latitudinal range of 50°S to 50°N globally from the year 2000.

[13] The Climate Prediction Center Morphing method (CMORPH) data set uses exclusively PMW estimates derived from the low-orbit SSM/I, TRMM, AMSU and AMSR-E satellites. Using a histogram matching method, the different PMW records are calibrated with TMI and subsequently their main features are transported to areas without coverage using spatial information derived from IR data. This method allows denser space-time precipitation coverage. The shape and intensity of precipitation at each location is calculated using a morphing mechanism that performs time-weighted interpolation between two successive PMW estimates that have been propagated forward and backward in time. CMORPH data are available every 3 h at a 0.25-degree resolution covering a region located between 60°N and 60°S starting in December 2002 [*Joyce et al.*, 2004].

[14] Daily observed precipitation was obtained from an extended rain gauge network put in place from 15 November 2002 to 15 February 2003 during the South American Low Level Jet Experiment (SALLJEX) [*Vera et al.*, 2006]. During SALLJEX more than 795 rain gauges where installed in SESA and more than 1500 were made available for the special network in a region where existing surface observations are insufficient. The precipitation database has undergone preliminary quality control by the Atmospheric Sciences Department at the Universidad de Buenos Aires and has been used in previous studies by *Rozante and Cavalcanti* [2008]. In order to facilitate our analysis, daily precipitation totals reported at 12 UTC were regridded to a common 0.25-resolution grid using a linear interpolation. Table 1 shows the results of the sensitivity analysis of CRA model parameters and number of grid points to changes in the Interpolation method. Three methods were tested on the storm registered on 23 December 2002 (Figure 2): triangle-based linear (linear), triangle-based cubic (cubic) and nearest neighbor. Parameter values range from 39.5 to 43.2 mm/d for average rainfall rate, from 140.0 to 153.0 mm/d for maximum rainfall, from 17.7 to 18.7 km^3 for rainfall volume, and from 503 to 543 for the number of grid points. For each model parameter, we computed the deviation from the Linear method, defined as

Table 1. Sensitivity Analysis of the Interpolation Method Used for Observed Precipitation

	Average Rainfall Rate	Maximum Rainfall	Rainfall Volume	Grid Points
Linear	39.5 mm/d	140.7 mm/d	17.7 km^3	543
Cubic	40.1 mm/d	153.0 mm/d	18.3 km^3	529
Nearest neighbor	43.2 mm/d	140.0 mm/d	18.7 km^3	503
Deviation from linear	9.3%	8.7%	5.6%	7.3%

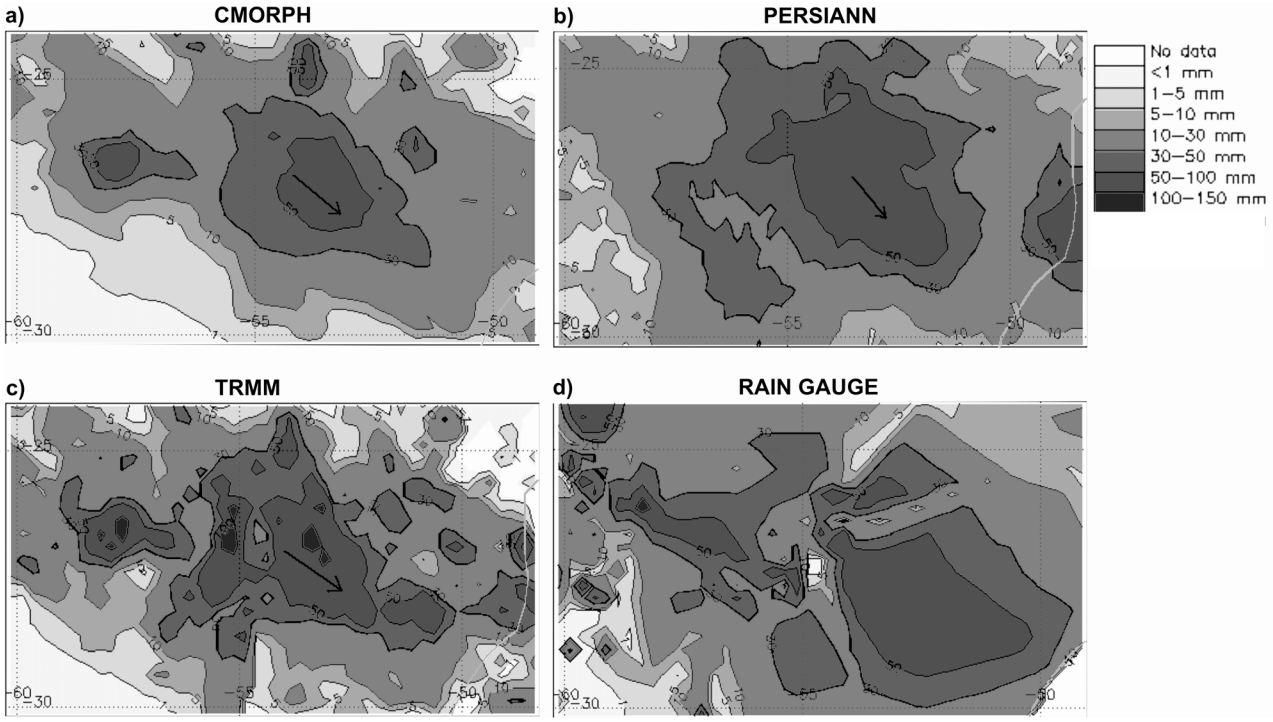

Figure 2. MCS event observed on 23 December 2002 over the La Plata River basin for (a) CMORPH, (b) PERSIANN, (c) TRMM, and (d) rain gauge. The heavy line shows the boundary of the CRA delineated with the 30 mm isohyet. The arrow shows the displacement of the satellite-estimated storm in the northwest position.

the difference between the largest or smallest parameter value obtained with the cubic or nearest neighbor method and with the Linear method, and normalized by the later. The largest deviation was found to be 9.3% for the average rainfall rate whereas for maximum rainfall, rainfall volume and grid points the deviations were 8.7, 5.6 and 7.3%, respectively. These results indicate that the impact of the interpolation method on parameter values does not have an effect on the results of our study. Precipitation totals were computed for each satellite product by adding up 3- or 6-hourly satellite estimates depending on the product availability. The satellite products are to be referred hereafter as TRMM, CMORPH and PERSIANN and the ground precipitation measurements as observations.

3. Overview of the CRA Method and Methodology

[15] The CRA method was developed by *Ebert and McBride* [2000] with the aim of verifying to what extent the forecasted or estimated rain entity had the same location, shape and magnitude of the one that was observed. The CRA method defines entities or contiguous rain areas as the region bounded by a user-specified isohyet. First an entity is delineated in the satellite and the observed fields based on the selected threshold and then a displacement error is determined by incrementally moving the estimated field over the observed field until a best fit criterion is optimized. The total error in the satellite estimated field can be broken down as the sum of errors due to location, volume and pattern. However, occasionally the error decomposition obtained using this criterion gives rise to a negative displacement error in equation (1), for these cases the error decomposition introduced by *Grams et al.* [2006] is used instead. In our study eight storm events produced a negative displacement error and the correlation decomposition method was selected. The total mean square error (MSE) can be written as

$$MSE = MSE_{displacement} + MSE_{volume} + MSE_{pattern}, \qquad (1)$$

where $MSE_{displacement}$ represents the difference between MSE before and after the translation, MSE_{volume} is the difference in mean intensity between the original and the shifted fields multiplied by the number of grid points in the CRA, and $MSE_{pattern}$ accounts for differences in the fine structure of both fields, i.e., the satellite product incorrectly representing the detailed rain structure such as satellite precipitation showing more detail or the precipitation maximum positioned in a different location.

[16] Second, each of the satellite products was paired with the observations and a visual inspection was performed to verify that the system was detected in both fields, i.e., observed and satellite-estimated. Third, the CRA method was used to analyze each set of observed and satellite-derived precipitation fields. The statistical significance of the correlation coefficient being different to zero at a 95% confidence level was tested using the F test [*Ebert and McBride*, 2000]. Finally, for each satellite product the differences between satellite-estimated and observed pre-

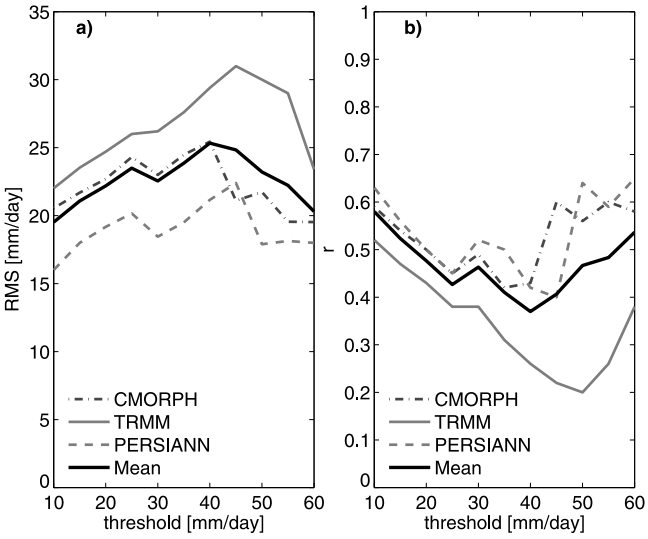

Figure 3. Sensitivity analysis of CRA precipitation threshold parameter for the MCS event registered on 23 December 2002. (a) RMSE in mm/d for three satellite products: CMORPH, TRMM, PERSIANN, and mean. (b) Same as in Figure 3a but for the correlation coefficient r.

cipitation parameters were measured using the bias. The mathematical expression for the bias is

$$bias = \sum_{i=1}^{n} (Sat_i - Obs_i), \tag{2}$$

where Sat_i denotes the satellite-estimated precipitation and Obs_i denotes observed precipitation in each grid box i.

[17] Figure 2 shows a four-panel plot with an example of CRA verification for a typical event recorded on 23 December 2002 for CMORPH, PERSIANN, TRMM, and observations. This event had an average life span and area. A displacement vector (black arrow) denotes the shifting of the satellite field to match the observed field by maximizing the correlation coefficient between both entities. Note that the size of the verification domain encloses the raining grid points and can be different for every satellite product.

[18] A macroscale hydrological model was used to evaluate how uncertainty in the spatial location of the storm propagated through the hydrological cycle. For this purpose, synthetic precipitation fields were generated for the Iguazu basin by incrementally shifting the observed precipitation along a latitudinal transect. The reader is referred to section 5 for details of the hydrological model used in the study. The hydrological model performance was evaluated with the Nash-Sutcliffe efficient (NSE) coefficient as

$$NSE = 1 - \frac{\sum_{i=1}^{n} (Sim_i - Obs_i)^2}{\sum_{i=1}^{n} (Obs_i - \mu_o)^2}, \tag{3}$$

where Sim_i denotes the streamflows simulated with the hydrological model using observed precipitation and Obs_i denotes observed streamflows at the basin's outlet, μ_o is the mean of the observations, and n is the number of values in the streamflows record.

4. Detecting Systematic Errors in Satellite Precipitation

[19] The CRA method requires the specification of three parameters: the precipitation threshold which is the isohyet used to isolate precipitation entities, i.e., grid points where rain intensities are larger than the threshold and are to be included in a CRA. This threshold is critical for the inclusion or division of multiple rain entities in a CRA and effectively selects those precipitation values for which the statistics are computed. In the United States and Australia, parameter values of 6.35 mm/6 h and 20 mm/d were adopted by *Grams et al.* [2006] and *Ebert and McBride* [2000], respectively. Decreases in the magnitude of the threshold allow the inclusion of smaller entities with the drawback of partitioning events into unrealistically small entities. A sensitivity analysis of the threshold parameter was performed for the typical event shown in Figure 2. Parameter values in the 10 to 60 mm/d range were used in the analysis. Figure 3 shows the impact of different parameter values on RMS and correlation coefficient between observed and satellite-estimated MCS that occurred on 23 December 2002. Mean RMS values range from 20 to 25 mm/d increasing with larger threshold values and reaching a maximum at around 40 mm/d. Conversely, the correlation coefficient ranges from 0.38 and 0.58 for the mean of the three satellites and reaches a minimum of 0.38 for the 40 mm/d threshold value. Model performance is more sensitivity to small and large threshold values for which RMS and r take the smallest and largest values, respectively. However, threshold values located in the lower end of the feasible range forces the CRA model to combine individual observed systems into one large CRA; on the other hand a threshold located in the upper end of the feasible range does not include parts of the storm in the analysis and statistics are calculated over an area that is not representative of the MCS. Performance measures remain stable in the 20–40 mm/d parameter range indicating that changes in the threshold value does not affect the outcome of the CRA method. Based on the results of the sensitivity analysis, and the magnitude of the storms in the basin, whose maximum intensity surpasses 100 mm/d; a threshold of 30 mm/d was chosen for the study. This threshold value produced reasonable looking entities for MCSs in the basin.

[20] The second user-defined parameter is the critical mass threshold, which defines the minimum volume of rainfall necessary for a system to be identified. The area of the smallest MCSs was found to be approximately 55,000 km^2 at the time of its maximum extension, which corresponds to a volume of 1.65 km^3 when a rainfall event of 30 mm/d is considered. Since increases of the critical mass might have excluded smalls systems we chose to use the default value of 1 km^3. A sensitivity analysis of the critical mass parameter indicated that increases in the magnitude of this parameter resulted in less entities being identified and the exclusion of small MCSs (not shown). Finally the search radius, which allows the separated observed and estimated rain entities to be compared, as long as they are within the search limit, was set to the default

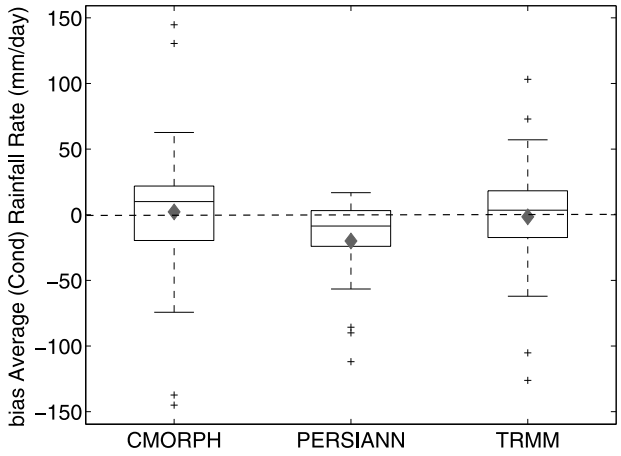

Figure 4. Box plot of bias (satellite-estimated minus observed) in average (conditional) rainfall rate in mm/d for CMORPH, PERSIANN, and TRMM satellite products. The bottom and top lines represent the 25th and 75th percentiles, and the middle line represents the median. The mean is indicated by the gray diamond. Whiskers extend from each end of the box to the adjacent values in the data within 1.5 times the interquartile range. The interquartile range is the difference between the third and the first quartile, i.e., 25th and 75th percentiles. Outliers are displayed with pluses.

value of six grid points in all directions. This represents a search radius of approximately 558.5 km over which the satellite-estimated system could be moved to match the observed rain entity.

[21] Daily observed precipitation was plotted for the days when a MCS was reported in order to check if those events identified with IR satellite imagery by *Salio et al.* [2007] were also captured by the surface network. The position of the storm's centroid was used to visually locate a system in both precipitation fields; only those systems that were simultaneously reported in the four fields (i.e., three satellite products and observations) were included in the analysis. By doing this, those events detected by the satellite product but not observed (false alarms) and alternatively those observed but not estimated (missed events) were eliminated. This process significantly reduced the numbers of MCSs to be examined from over one hundred to twenty-four (Figure 1). Note that some events had lifecycles of up to 42 h, for those cases with lifecycles exceeding a day only the cumulative precipitation for the day where the maximum extension occurred was used. The substantial reduction in the number of MCSs included in the study was partially caused by a decline in the number of reporting stations over the El Pantanal region, in the northwest corner of the basin, by the existence of adjacent systems, which in several occasions overlaid making difficult the demarcation of one system, and by missing data in CMORPH and PERSIANN archives. No significant differences to the eye of the human forecaster were found in the performance of the CRA method when the RMSE or the correlation coefficient between the fields was used as a matching criterion (not shown). The correlation coefficient tends to match observed and estimated precipitation gradients rather than precipitation peaks hence it can more efficiently measure the matching between moving storm cells. Based on this, the matching criterion used to compute spatial displacements was the maximization of the correlation coefficient, and the error decomposition was based on the MSE (equation (1)), which had shown to give more robust error components [*Ebert and Gallus*, 2009].

[22] Statistics were calculated for the following parameters: average (conditional) rainfall rate, rainfall volume, maximum rainfall, and displacement. Additionally the total error decomposition into the three components of displacement, volume, and pattern error, (equation (1)) was computed.

4.1. Average Rainfall Rate

[23] Figure 4 shows box plots of bias in average (conditional) rainfall rate, i.e., nonzero rainfall rates above the selected threshold, for CMORPH, PERSIANN and TRMM precipitation estimates. CMORPH estimates show a wet (positive) bias in the median with a value of 10 mm/d and extreme values as large as ±150 mm/d which represents up to ±200% of the observed mean and it is considered quite large even for noisy satellites estimates [*Sapiano and Arkin*, 2009]. Over Australia, CMORPH satellite estimates have shown systematic positive biases for rain intensities exceeding the 20 mm/d threshold and over the continental United States there are clear indications that CMORPH presents large positive biases during the warm season, which is in agreement with our findings for South America [*Sapiano and Arkin*, 2009; *Ebert et al.*, 2007; *Tian et al.*, 2007]. Even though the sign of the bias is consistent in all the studies, the magnitude of the bias in our study is significantly larger due to the fact that we are focusing only on heavy rain events hence the differences between ground and remotely sensed precipitation is amplified. From a hydrologic standpoint these biases can affect fast-response processes in the basin such as Hortonian infiltration, soil compaction, or canopy interception, which can result in changes in the rainfall-runoff response. However, due to the lack of subdaily observed precipitation assessing the magnitude of these impacts is outside the scope of this paper.

[24] PERSIANN rainfall estimates on the other hand show a strong tendency to underestimate the average rainfall rate with a median value of −8.5%. Despite showing an overall dry bias, the discrepancy in the values is smaller for PERSIANN estimates with extremes values ranging from −100 to 25% of the observed values. These results disagree with studies of daily precipitation in the United States, South America and Australia [*Sapiano and Arkin*, 2009; *Ebert et al.*, 2007; *de Goncalves et al.*, 2006] who found a systematic overestimation of daily estimates by PERSIANN products.

[25] Of all the satellite products considered in this study, only TRMM has a bias correction applied at a monthly scale using ground-based precipitation. The median of average rainfall Rate estimated by TRMM has a small positive bias (3 mm/d) indicating that the gauge correction does offer a significant advantage over other uncorrected satellite products for an accurate representation of MCSs in SESA. It is worth mentioning that a large number of rain gauges used in this study are not routinely available for TRMM ground validation and calibration constituting an independent validation source.

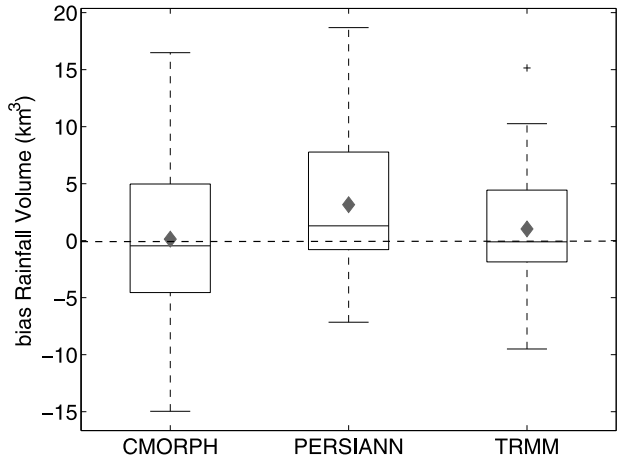

Figure 5. Same as Figure 4 but for rainfall volume in km^3.

4.2. Rainfall Volume

[26] Figure 5 shows the bias in unconditional rainfall volume in km^3 for the three satellite products. Unconditional rainfall was selected to compare observed and satellite precipitated volumes over a common area. CMORPH and TRMM show unbiased medians, however biases in storm volume range from −15 to 15 km^3 in the case of CMORPH and slightly less in the case of TRMM (−10 to 10 km^3); these differences represent as much a ±100% of the mean observed volume for all the recorded events. PERSIANN overestimates volumes for almost all the storms with a median value of 1.3 km^3 and extremes between −7 and 18 km^3 (−50 to 140% of the observed volume). This is surprising since the average rainfall rate and rainfall volume are closely related parameters therefore the same sign in the bias is expected. PERSIANN shows systematically larger storm areas than observations, which significantly reduces the conditional average rainfall rate (Figure 4). Conversely when unconditional rainfall is considered, e.g., zero and nonzero pixels, more spatially extended storms yield a larger rainfall volume.

[27] Table 2 shows the number of 0.250° grid points exceeding the 30 mm/d threshold for the three satellite products and the observational network. The average size of MCSs for CMORPH and TRMM is below 20% of the observed size. Conversely PERSIANN has a large positive bias (90% of the observed storm size) indicating a systematic overestimation of the storm area. This reflects that the adaptive neural network calibration of IR imaginary is not capturing the spatial extension of the convective events.

Table 2. Summary of Average MCS Sizes From Satellite Precipitation Products[a]

Satellite	Storm Average Size (Number of Grid Points)	Bias (%)
CMORPH	257	−1.2
PERSIANN	494	90.0
TRMM	314	20.8

[a]The bias is expressed as a percentage of the ground observed size.

4.3. Maximum Rainfall

[28] The highest observed precipitation amount in any of the 0.25-degree cells included in the verification domain is considered to be the maximum rainfall for a MCS (Figure 6). CMORPH and PERSIANN underestimate the maximum rain with a median of −12 and −16 mm/d, respectively, and values ranging ± 100% of the observed values. The TRMM product overestimates observed maximum rainfall with a median bias value of +14 mm/d (32% of the observed mean). This indicates that the monthly bias correction efficiently corrects total precipitation amounts but does filter high-intensity events such as those generated for a MCS. These findings are in agreement with the results of *Tian et al.* [2007], for the United States, who found that TRMM estimates detected stronger precipitation events than observations causing a shift in the precipitation spectrum toward higher rainfall intensities.

4.4. Displacements in the Location of the MCSs

[29] The spatial distribution of errors in the location of MCSs are displayed in a x-y plot where negative values represent displacements from the center of mass of the observed event in the south and west directions, and positive values represent displacements in the east and north directions. The CRA method looks at all possible displacements within the search box and chooses the one that gives the maximum correlation or minimum RMSE, depending on which matching criterion has been specified by the user. Figure 7 shows the location of the centroids for each satellite product within a 5-degree radius. Dispersion is high for the three satellite products with storm centroids displaced as far as 500 km from the location of the observed event. Each individual storm was visually inspected to verify that the magnitude of the error obtained with the CRA method was in close agreement with the error detected by the human eye.

[30] All three satellite products showed a preferential direction of displacement along an east-west transect with TRMM and CMORPH having less dispersion in the longitudinal direction than PERSIANN (Figures 7a and 7c). This behavior is in part consistent with the findings of *Velasco*

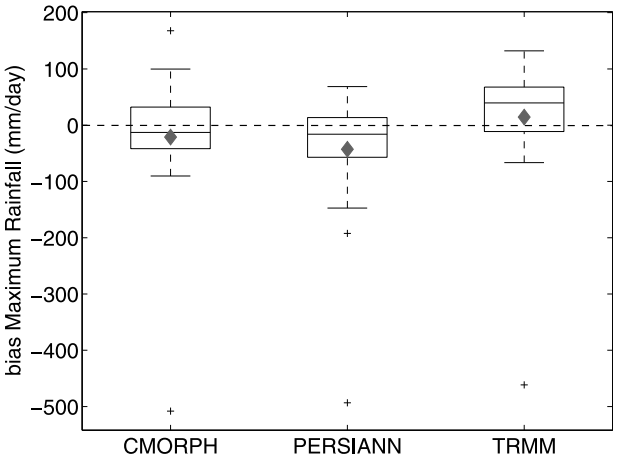

Figure 6. Same as Figure 4 but for maximum rainfall in mm/d.

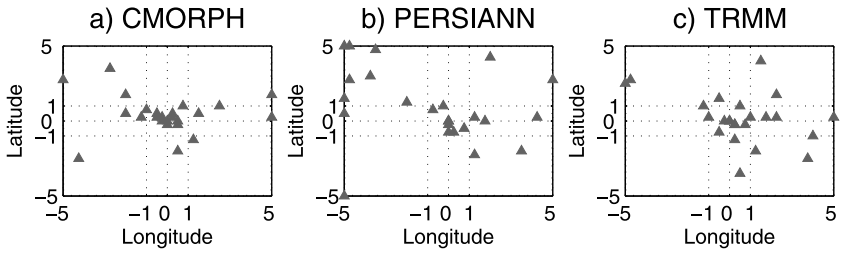

Figure 7. Displacement of satellite-estimated MCSs with respect to observed systems. The *x* and *y* axes represent longitude and latitude in degrees, respectively. (a) CMORPH, (b) PERSIANN, and (c) TRMM.

and Fritsch [1987] for Meso Convective Complexes in the region who found the tracks of these systems had a general pattern of migration from west to east. Displacements in PERSIANN showed the largest dispersion with storm locations distributed almost equally in the northeast, northwest and southeast directions (Figure 7b). One possible explanation to the errors in the location of the systems could be due to the fact PERSIANN relies on IR data to estimate rainfall therefore satellite sensors can only detect convective precipitation from cold cloud tops consequently not detecting rainfall precipitating from warm shallow clouds [*Ebert et al.*, 2007]. Only the CMORPH algorithm attempts to account for rain system movement by means of the morphing procedure. Another factor that could be affecting the location of the storms is related to the fact that if precipitation reaches its maximum between two consecutive satellite overpasses, the satellite cannot detect it and the system's migration is not fully described by satellite products.

4.5. Error Decomposition

[31] One of the main features of the CRA method is the possibility to represent the total error as the sum of the error due to displacements, the error in volume and the error due to small differences in the structure of the estimated and observed storms (pattern error). Figure 8 shows the average contribution to the total error of each error component for the three satellite products. For CMORPH rainfall estimates, on average the major source of error arose from discrepancies in the small structure of the storm totaling more than 50% of the total error followed by errors in volume (Figure 8a). The pattern error is strongly influenced by spatial variability that can be a function of the type of sensor, satellite spatial and especially temporal sampling, and the retrieval algorithm used to generate the estimates. For PERSIANN, errors in pattern contributed to 61% of the total error whereas errors in volume and displacement represented 15 and 24% of the total error, respectively (Figure 8b). In TRMM estimates the largest contribution to the total error came from differences in the fine structure between fields, which contributed to 65% of the total error. Errors in volume and displacement represented 20 and 15% of the total error, respectively.

5. Case Study: Evaluating the Impact of Displacement Errors on Streamflow Simulations

[32] When considering the usefulness of satellite-estimated precipitation for hydrological applications, it is crucial to consider the impact that errors in the location of the storm has on streamflow properties mainly the peak. In recent years, a number of studies have looked at the effects of the spatial variability of rainfall on simulated peaks and they have concluded that it can play a major role in the uncertainty of streamflows in a basin [*Younger et al.*, 2009; *Carpenter and Georgakakos*, 2004; *Arnaud et al.*, 2002; *Wilson et al.*, 1979]. In addition, published studies have examined the influence of storm movement, as well as the position of the storm centroid, on overland flow [e.g., *Chang*, 2007; *Morin et al.*, 2006; *Syed et al.*, 2003; *de Lima and Singh*, 2002]. The studies concluded that the position of the storm core relative to the watershed outlet becomes more important as the catchment size increases and that upstream moving storms generate smaller peaks than downstream moving storms. However, these studies are restricted to small basins and to precipitation products derived from radar measurements therefore an evaluation of the effects of storm

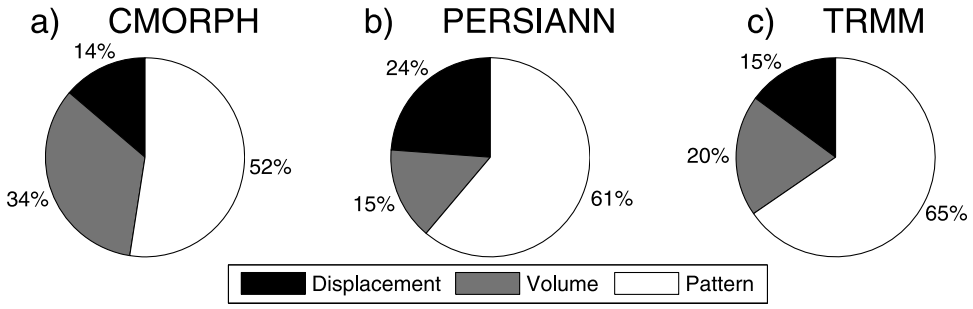

Figure 8. Decomposition of the total error into its sources: displacement, volume, and pattern. (a) CMORPH, (b) PERSIANN, and (c) TRMM.

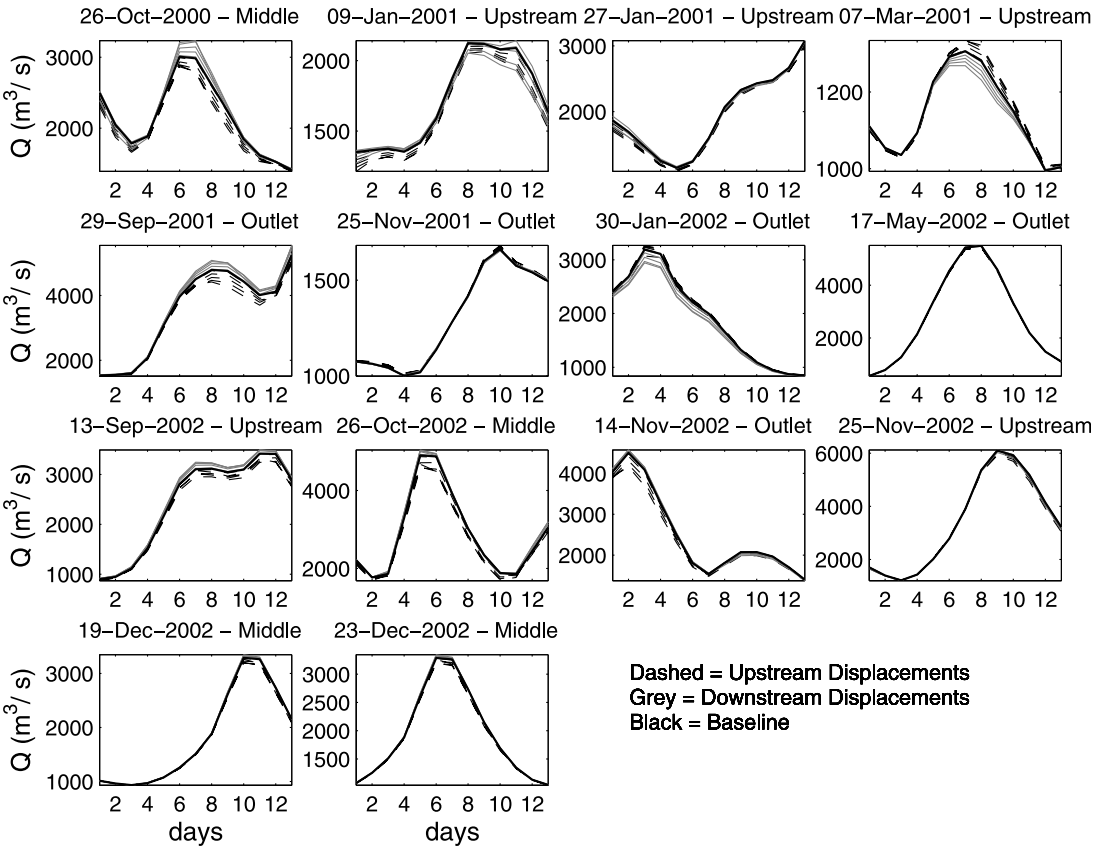

Figure 9. Daily streamflows at Estreito station for 12 days after the occurrence of a MCS in the basin. The black line represents baseline streamflows simulated with error-free precipitation, and the dashed/gray lines represent streamflows simulated with shifted precipitation upstream/downstream. Above each plot is the day of the MCS and the spatial location at the time of its maximum development.

location is lacking. To evaluate how this type of error affects the different components of the hydrologic cycle, a small subbasin of the La Plata basin was selected as a case study: the Iguazu river basin. The Iguazu Basin is a transboundary watershed located in southeastern part of the La Plata Basin (Figure 1). The basin has an area of approximately 70,000 km^2 and is located between 25°S and 27°S and 49°W and 55°W. From its headwaters in Brazil at 1400 m of altitude, the river flows east-west for approximately 1300 km until its confluence with the Paraná river in Argentina.

[33] The hydrological cycle in the Iguazu river basin was represented with the variable infiltration capacity (VIC) model. VIC is a macroscale hydrologic model that has the capability to represent the sub-grid-scale variability of vegetation coverage, topography, precipitation and soil moisture storage capacity. For details of VIC mathematical formulations the reader is referred to *Liang et al.* [1994, 1996]. The VIC formulation for the Iguazu basin uses three soil layers of 0.1, 1.5 and 1.0 m of thickness from top to bottom, and 9 vegetation types. VIC was implemented at a daily time step and a spatial resolution of 0.125 degrees. Although a finer temporal resolution would have been desirable to be able to detect subdaily streamflow behavior only daily records of precipitation and streamflows were available for the basin. VIC was run in water balance mode (VIC Version 4.0.6). A data set of daily total precipitation for the Iguazu basin was available for the period 1 January 1979 to 31 December 2005 at a 0.25-degree resolution [*Liebmann and Allured*, 2005]. This data set does not incorporate the additional rain gauges put in place during SALLJEX in the central west part of the LPB but it offers an excellent spatial coverage over the Iguazu Basin for an extended period of time. Maximum and minimum daily temperatures and wind fields were obtained from the National Center for Environmental Prediction (NCEP) Reanalysis 2 available at 2.5-degree resolution [*Kanamitsu et al.*, 2002]. Meteorological forcings were interpolated to a 0.125-degree resolution using a linear scheme. Daily streamflows at Estreito Station (−25,55°S, −53.80°W) were obtained from the Brazilian National Water Agency (ANA) (http://www.ana.gov.br/) and used to evaluate the model's performance. VIC streamflow simulations, driven with observed fields, were considered the "truth" and used to compute errors between shifted and baseline model simulations. For more information on the implementation and performance of VIC in the Iguazu basin the reader is referred to E. M. Demaria et al. (Evaluating the propagation of errors in satellite precipitation estimates to hydrological applications in South America, manuscript in preparation, 2011).

[34] Synthetic error-perturbed precipitation fields were generated by displacing the observed precipitation along the east-west direction. This direction was chosen following the

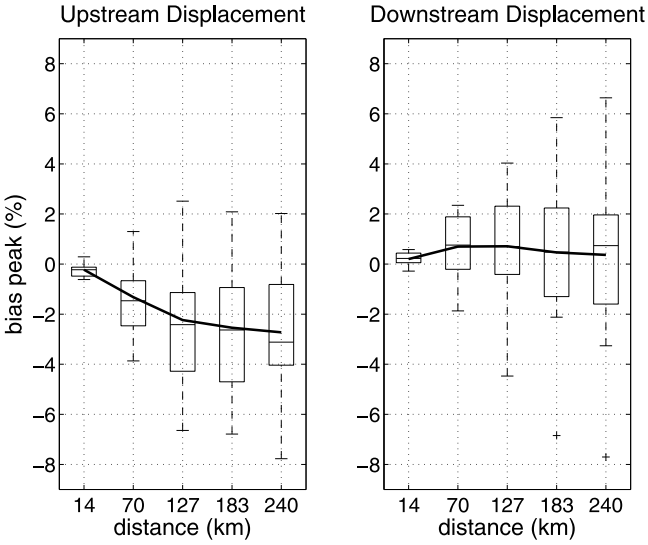

Figure 10. Bias between peaks simulated with shifted and unshifted precipitation as a percent of the baseline flow. (left) Results with upstream displacements along a latitudinal transect and (right) results for downstream displacements. The line shows the median.

results presented in Figure 7, which indicated that displacement errors in satellite-estimated precipitation tended to be dominant along a latitudinal transect. Observed precipitation fields were incrementally moved upstream/downstream (eastward/westward) 14.125, 70.625, 127.125, 183.625 and 240.125 km. Even though the maximum displacement is smaller than the maximum found in Figure 7, it is representative of the displacements experienced by the majority of the systems. The other atmospheric forcings used in the model, i.e., temperature and wind, remained the same as in the baseline simulations.

[35] During the period 1 September 2000 to 31 May 2003, fourteen MCSs were identified in the Iguazu Basin using a tracking algorithm applied to IR satellite imagery [*Vila et al.*, 2008; *Salio et al.*, 2007]. The systems varied in size from 76,400 to 505,260 km^2 (mean areal size: 193,340 km^2), they initiated in average at 1700 UTC and ended at 0300 UTC of the next day reaching the maximum extension at 2000 UTC. At the time of their maximum extension, the geographical positions of the systems where centered in the upper basin (five systems), middle basin (four systems) and lower basin (five systems) (refer to Figure 1 for the locations of the systems). The average life span of a MCS was nine and a half hours with the events located in the upper basin being relatively shorter in duration. Figure 9 shows daily streamflows at the basin's outlet for the twelve consecutive days after an MCS was identified in the basin. Note that the basin's response time is approximately 5 days between the headwaters and the outlet. The streamflows simulated with shifted precipitation generally undergo increases/decreases in the magnitude of the flows' downstream/upstream displacements. For almost all the events analyzed the dispersion is larger in the proximity of the peak than in the rising limb and the recession. Despite changes in the magnitude of the flows, the timing of the peaks is not affected by shifts in precipitation. This behavior indicates that in large-size basins, such as the Iguazu basin, the effects of storm moving further away from the mouth can flatten the peak as a result of channel storage. For storms mowing downstream the increase in the peak is due to rainfall at the mouth concurrent with streamflow contributions from the upper part of the basin. Changing the location of the storm had practically no effect on the timing of the peak indicating that for large-size basins the surface storage and the channel network can lessen the impact of this type of error. Another contributing factor is the daily discretization of the VIC model, which does not allow capturing the subdaily variability of streamflows in the basin.

[36] The impact of systematic displacement of precipitation on the peak of the hydrograph is shown in Figure 10. The bias, as a percentage of the baseline peak, is computed between the error-free peak and the peak of the event simulated with precipitation moved upstream and downstream the basin. Simulations with precipitation shifted in the upstream direction systematically underestimate error-free peaks indicating a smoothing in the response of the system. For displacements in the downstream direction simulated peaks overestimated baseline peaks as the result of increasing runoff contribution. This is valid for daily time scales when additional smoothing is introduced by the temporal averaging of short-term fluctuations. Despite the change in the sign of the bias, the magnitude of the differences is quite small not surpassing a five percent difference from the baseline peak. These results indicate that for a basin of the size of the Iguazu and for a daily time step, errors in the location of a satellite-estimated MCS do not have a significant impact on hydrological applications that require a precise estimate of the peak magnitude. Furthermore, if one considers that the error associated with streamflow measurements using a rating curve can be, in average, as large as 25%, the increment of peak discharge due to displacement in precipitation can be considered almost negligible for a large-scale basin [*Di Baldassarre and Montanari*, 2009].

6. Conclusions

[37] The ability of three satellite products to represent the spatial characteristics of MCSs over the La Plata River basin in southeastern South America was examined with an object-based approach, the CRA method. This method allows for the objective determination of the source of errors affecting the correct characterization of storm events in space and time, verification that cannot be made with traditional grid-to-grid techniques. During the austral summer 2002–2003, precipitation events exceeding 30 mm/d for three satellite products: TRMM, CMORPH and PERSIANN were evaluated against observed precipitation, which was considered the benchmark. The analysis of the different statistical parameters provided by the CRA method indicated the existence of systematic deficiencies in the three satellite products representing convective system over the basin. The impact of the location of the storm on basin streamflows was evaluated by forcing a macroscale hydro-

logical model with spatially shifted precipitation fields. The main conclusions of our investigation are as follows:

[38] 1. The average (conditional) rainfall rate of MCSs, delineated with the 30 mm/d isohyet, shows significant dispersion for all satellite products. CMORPH overestimates ground observations whereas PERSIANN estimates are systematically smaller than observations. TRMM median average rainfall rate is unbiased confirming that the bias correction performed at the monthly level effectively increases the accuracy of the estimates.

[39] 2. The spatial extension of MCSs is overestimated by PERSIANN causing a systematic dry bias in the average conditional rainfall rate. The PERSIANN tendency to underestimate average rainfall rate may be result from IR measurements misclassifying cirrus clouds as precipitating systems. Further studies are needed to quantify these effects.

[40] 3. Both CMORPH and TRMM successfully capture the median of the storm volume over the basin whereas PERSIANN slightly overestimates observations. Hence some hydrological applications that require an estimation of the amount of water in the channel, e.g., water supply, will be more sensitive to errors in satellite-estimated precipitation.

[41] 4. The maximum rainfall of the storm is better captured by CMORPH and PERSIANN, which are the two satellite-only products included in the study, nevertheless intense rainfall rates are systematically smaller than observed ones. TRMM on the other hand overestimates intense rainfall despite being bias-corrected with ground observations indicating that the correction procedure does not filter some of the noise existing in the data.

[42] 5. The preferential direction displacement of satellite-estimated MCSs is in the east-west direction for CMORPH and TRMM resembling the trajectory of some mesoscale systems in the region. PERSIANN estimates showed displacements equally distributed in the northeast, northwest and southeast directions.

[43] 6. Discrepancies in the fine structure of the storms dominate the total error decomposition of all satellite products. For TRMM estimates, this source of error represents more than 65% of the total error whereas errors in displacement and volume are small resulting from the ground-based bias correction routinely performed. The contribution to the total error from errors in volume is small for PERSIANN estimates whereas they are significant for CMORPH products.

[44] 7. Hydrological simulations of streamflows in the Iguazu basin indicate that the location of the storm influences the magnitude of the peak, hence its volume, when it is shifted upstream and downstream the basin. Displacements in the location of a satellite-estimated MCS does not have a significant impact on the timing of the peaks indicating that the basin's response to precipitation diminishes the effect that errors in storm location has on simulated streamflows.

[45] As previous studies pointed out, the incorporation of rain gauge information in TRMM not surprisingly reduces the bias in the storm volume and average rainfall rate [*Tian et al.*, 2007]. However, for intense rainfall rates there is not clear gain over satellite products that are not bias-corrected, which along with the latency in availability reduces its applicability in real time rainfall-runoff applications such as flash flood warning. Unfortunately, the real time operational version of TRMM was not available at the time of SALLJEX and was not included in this study.

[46] CMORPH estimates, which are entirely based on remotely sensed measurements without a ground-based correction, performed equally well for rainfall volume and even outperformed TRMM detecting the maximum rainfall indicating that the "morphing" method used can successfully capture the spatial characteristics of large convective systems.

[47] The results of this study are valid for convective storm that exceed the 30 mm/d threshold and for rain dominated large-scale basins where saturation excess mechanisms are predominant. For subdaily temporal scales differences in peak arrival time might become significant. Questions remain regarding the accuracy of the satellite products at a subdaily time step and if some characteristics such as the onset and duration of the events are well captured. Unfortunately there is no indication that the density of the surface network will be improved in the near future leaving the fate of this type of analysis to future field campaigns.

[48] **Acknowledgments.** This study was funded by NASA PMM grant NNG04GA79G to the University of Arizona. This material is based upon work supported in part by SAHRA (Sustainability of semi-Arid Hydrology and Riparian Areas) under the STC Program of the National Science Foundation, agreement EAR-9876800. We would like to thank Jeremy S. Grams for his help in understanding the CRA method and Jonathan D. Whittier for his help with ArcGIS. Precipitation for the Iguazu basin was kindly provided by Brant Liebmann and David Allured at NOAA-CIRES Climate Diagnostics Center, Boulder, Colorado. The authors would like to thank the two anonymous reviewers for their valuable suggestions that led to substantial improvements to this work.

References

Arnaud, P., C. Bouvier, L. Cisneros, and R. Dominguez (2002), Influence of rainfall spatial variability on flood prediction, *J. Hydrol.*, *260*, 216–230, doi:10.1016/S0022-1694(01)00611-4.

Astin, I. (1997), A survey of studies into errors in large scale space-time averages of rainfall, cloud cover, sea surface processes and the Earth's radiation budget as derived from low Earth orbit satellite instruments because of their incomplete temporal and spatial coverage, *Surv. Geophys.*, *18*, 385–403, doi:10.1023/A:1006512715662.

Bell, T. L., and P. K. Kundu (2000), Dependence of satellite sampling error on monthly averaged rain rates: Comparison of simple models and recent studies, *J. Clim.*, *13*, 449–462, doi:10.1175/1520-0442(2000)013<0449:DOSSEO>2.0.CO;2.

Berbery, E. H., and V. R. Barros (2002), The hydrologic cycle of the La Plata Basin in South America, *J. Hydrometeorol.*, *3*, 630–645, doi:10.1175/1525-7541(2002)003<0630:THCOTL>2.0.CO;2.

Carpenter, T. M., and K. P. Georgakakos (2004), Impacts of parametric and radar rainfall uncertainty on the ensemble streamflow simulations of a distributed hydrologic model, *J. Hydrol.*, *298*, 202–221, doi:10.1016/j.jhydrol.2004.03.036.

Chang, C. (2007), Influence of moving rainstorms on watershed responses, *Environ. Eng. Sci.*, *24*(10), 1353–1360, doi:10.1089/ees.2006.0220.

de Goncalves, L. G. G., W. J. Shuttleworth, B. Nijssen, E. J. Burke, J. A. Marengo, S. C. Chou, P. Houser, and D. L. Toll (2006), Evaluation of model-derived and remotely sensed precipitation products for continental South America, *J. Geophys. Res.*, *111*, D16113, doi:10.1029/2005JD006276.

de Goncalves, L. G. G., et al. (2009), The South American Land Data Assimilation System (SALDAS) 5-yr retrospective atmospheric forcing datasets, *J. Hydrometeorol.*, *10*, 999–1010, doi:10.1175/2009JHM1049.1.

de Lima, J. L. M. P., and V. P. Singh (2002), The influence of the pattern of moving rainstorms on overland flow, *Adv. Water Resour.*, *25*, 817–828, doi:10.1016/S0309-1708(02)00067-2.

Di Baldassarre, G., and A. Montanari (2009), Uncertainty in river discharge observations: A quantitative analysis, *Hydrol. Earth Syst. Sci.*, *13*, 913–921, doi:10.5194/hess-13-913-2009.

Doswell, C. A., III, H. E. Brooks, and R. A. Maddox (1996), Flash flood forecasting: An ingredients-based methodology, *Weather Forecast.*, *11*, 560–581, doi:10.1175/1520-0434(1996)011<0560:FFFAIB>2.0.CO;2.

Durkee, J. D., and T. L. Mote (2009), A climatology of warm-season mesoscale convective complexes in subtropical South America, *Int. J. Climatol.*, doi:10.1002/joc.1893.

Durkee, J. D., T. L. Mote, and J. Marshall Shepherd (2009), The contribution of mesoscale convective complexes to rainfall across subtropical South America, *J. Clim.*, *22*, 4590–4605, doi:10.1175/2009JCLI2858.1.

Ebert, E. E., and W. A. Gallus (2009), Toward better understanding of the contiguous rain area (CRA) method for spatial forecast verification, *Weather Forecast.*, *24*, 1401–1415, doi:10.1175/2009WAF2222252.1.

Ebert, E. E., and J. L. McBride (2000), Verification of precipitation in weather systems: Determination of systematic errors, *J. Hydrol.*, *239*, 179–202, doi:10.1016/S0022-1694(00)00343-7.

Ebert, E. E., J. E. Janowiak, and C. Kidd (2007), Comparison of near real-time precipitation estimates from satellite observations and numerical models, *Bull. Am. Meteorol. Soc.*, *88*, 47–64, doi:10.1175/BAMS-88-1-47.

Gilleland, E., D. Ahijevych, B. G. Brown, B. Casati, and E. E. Ebert (2009), Intercomparison of spatial forecast verification methods, *Weather Forecast.*, *24*, 1416–1430, doi:10.1175/2009WAF2222269.1.

Grams, J. S., W. A. Gallus Jr., S. E. Koch, L. S. Wharton, A. Loughe, and E. E. Ebert (2006), The use of a modified Ebert-McBride technique to evaluate mesoscale model QPF as a function of convective system morphology during IHOP 2002, *Weather Forecast.*, *21*, 288–306, doi:10.1175/WAF918.1.

Hirschboeck, K. K., L. Ely, and R. A. Maddox (2000), Hydroclimatology of meteorologic floods, in *Inland Flood Hazards: Human, Riparian and Aquatic Communities*, edited by E. Wohl, pp. 39–72, Cambridge Univ. Press, Cambridge, U. K., doi:10.1017/CBO9780511529412.003.

Hsu, K., X. Gao, S. Sorooshian, and H. Gupta (1997), Precipitation estimation from remotely sensed information using artificial neural networks, *J. Appl. Meteorol.*, *36*, 1176–1190, doi:10.1175/1520-0450(1997)036<1176:PEFRSI>2.0.CO;2.

Huffman, G. J. (1997), Estimates of root-mean-square random error for finite samples of estimated precipitation, *J. Appl. Meteorol.*, *36*, 1191–1201, doi:10.1175/1520-0450(1997)036<1191:EORMSR>2.0.CO;2.

Huffman, G. J., et al. (2007), The TRMM Multisatellite Precipitation Analysis (TMPA): Quasi-global, multiyear, combined-sensor precipitation estimates at fine scales, *J. Hydrometeorol.*, *8*, 38–55, doi:10.1175/JHM560.1.

Joyce, R. J., J. E. Janowiak, P. A. Arkin, and P. Xie (2004), CMORPH: A method that produces global precipitation estimates from passive microwave and infrared data at high spatial and temporal resolution, *J. Hydrometeorol.*, *5*, 487–503, doi:10.1175/1525-7541(2004)005<0487:CAMTPG>2.0.CO;2.

Kanamitsu, M., W. Ebisuzaki, J. Woollen, S.-K. Yang, J. J. Hnilo, M. Fiorino, and G. L. Potter (2002), NCEP-DEO AMIP-II Reanalysis (R-2), *Bull. Am. Meteorol. Soc.*, *83*, 1631–1643.

Kidd, C., V. Levizzani, J. Turk, and R. Ferraro (2009), Satellite precipitation measurements for water resource monitoring, *J. Am. Water Resour. Assoc.*, *45*(3), 567–579, doi:10.1111/j.1752-1688.2009.00326.x.

Liang, X., D. P. Lettenmaier, E. F. Wood, and S. J. Burges (1994), A simple hydrologically based model of land surface water and energy fluxes for general circulation models, *J. Geophys. Res.*, *99*, 14,415–14,428, doi:10.1029/94JD00483.

Liang, X., E. F. Wood, and D. P. Lettenmaier (1996), Surface soil moisture parameterization of the VIC-2L model: Evaluation and modifications, *Global Planet. Change*, *13*, 195–206, doi:10.1016/0921-8181(95)00046-1.

Liebmann, B., and D. Allured (2005), Daily precipitation grids for South America, *Bull. Am. Meteorol. Soc.*, *86*, 1567–1570.

Morin, E., D. C. Goodrich, R. A. Maddox, X. Gao, H. V. Gupta, and S. Sorooshian (2006), Spatial patterns in thunderstorm rainfall events and their coupling with watershed hydrological response, *Adv. Water Resour.*, *29*, 843–860, doi:10.1016/j.advwatres.2005.07.014.

Mota, G. V. (2003), Characteristics of rainfall and precipitation features defined by the Tropical Rainfall Measuring Mission over South America, Ph.D. dissertation, 215 pp., Meteorol. Dep., Univ. of Utah, Salt Lake City.

Nascimento, E. L., and C. A. Doswell III (2006), The need for an improved documentation of severe thunderstorms and tornadoes in South America, paper presented at Symposium on the Challenges of Severe Convective Storms, Am. Meteorol. Soc., Atlanta, Ga.

Nogués-Paegle, J., et al. (2002), Progress in pan American CLIVAR research: Understanding the South American monsoon, *Meteorologica*, *27*(1,2), 1–30.

Nunes, J. P., J. L. M. P. de Lima, V. P. Singh, M. I. P. de Lima, and G. N. Vieira (2006), Numerical modeling of surface runoff and erosion due to moving rainstorms and the drainage basin scale, *J. Hydrol.*, *330*, 709–720, doi:10.1016/j.jhydrol.2006.04.037.

Rodriguez, D. A., and I. F. A. Cavalcanti (2006), Simulations of the hydrological cycle over southern South America using the CPTEC/COLA AGCM, *J. Hydrometeorol.*, *7*, 916–936, doi:10.1175/JHM534.1.

Rozante, S. R., and I. F. Cavalcanti (2008), Regional Eta model experiments: SALLJEX and MCS development, *J. Geophys. Res.*, *113*, D17106, doi:10.1029/2007JD009566.

Salby, M. L., and P. Callaghan (1997), Sampling error in climate properties derived from satellite measurements: Consequences of undersampled diurnal variability, *J. Clim.*, *10*, 18–36, doi:10.1175/1520-0442(1997)010<0018:SEICPD>2.0.CO;2.

Salio, P., M. Nicolini, and E. J. Zipser (2007), Mesoscale convective systems over southeastern South America and their relationship with the South American low-level jet, *Mon. Weather Rev.*, *135*, 1290–1309, doi:10.1175/MWR3305.1.

Sapiano, M. R. P., and P. A. Arkin (2009), An intercomparison and validation of high-resolution satellite precipitation estimates with 3-hourly gauge data, *J. Hydrometeorol.*, *10*, 149–166, doi:10.1175/2008JHM1052.1.

Silva Dias, M. A. F. (1999), Storms in Brazil, in *Storms*, *Haz. Disasters Ser.*, vol. II, edited by R. Pielke Sr. and R. Pielke Jr., Eds., pp. 207–219, Routledge, Boca Raton, Fla.

Singh, V. P. (1997), Effect of spatial and temporal variability in rainfall and watershed characteristics on stream flow hydrograph, *Hydrol. Processes*, *11*, 1649–1669, doi:10.1002/(SICI)1099-1085(19971015)11:12<1649::AID-HYP495>3.0.CO;2-1.

Singh, V. P. (2002a), Effect of the duration and direction of storm movement on infiltrating planar flow with full areal coverage, *Hydrol. Processes*, *16*, 1479–1511, doi:10.1002/hyp.358.

Singh, V. P. (2002b), Effect of the duration and direction of storm movement on infiltrating planar flow with full and partial areal coverage, *Hydrol. Processes*, *16*, 3437–3466, doi:10.1002/hyp.1109.

Stanski, H. R., L. J. Wilson, and W. R. Burrows (1989), Survey of common verification methods in meteorology, *WMO/TD 358*, World Meteorol. Org., Geneva, Switzerland.

Su, F., H. Yang, and D. P. Lettenmaier (2008), Evaluation of TRMM Multi-satellite Precipitation Analysis (TMPA) and its utility in hydrologic prediction in La Plata Basin, *J. Hydrometeorol.*, *9*, 622–640, doi:10.1175/2007JHM944.1.

Syed, K. H., D. C. Goodrich, D. E. Myers, and S. Sorooshian (2003), Spatial characteristics of thunderstorm rainfall fields and their relation to runoff, *J. Hydrol.*, *271*, 1–21, doi:10.1016/S0022-1694(02)00311-6.

Teixeira, M. S., and P. Satyamurty (2007), Dynamical and synoptic characteristics of heavy rainfall episodes in southern Brazil, *Mon. Weather Rev.*, *135*, 598–617, doi:10.1175/MWR3302.1.

Tian, Y., C. D. Peters-Lidard, D. J. Choudhury, and M. Garcia (2007), Multitemporal analysis of TRMM-based precipitation products for land data assimilation applications, *J. Hydrometeorol.*, *8*, 1165–1183, doi:10.1175/2007JHM859.1.

Velasco, I., and J. M. Fritsch (1987), Mesoscale convective systems in the Americas, *J. Geophys. Res.*, *92*, 9591–9613, doi:10.1029/JD092iD08p09591.

Vera, C., et al. (2006), The South American Low-Level Jet Experiment, *Bull. Am. Meteorol. Soc.*, *87*, 63–77, doi:10.1175/BAMS-87-1-63.

Vila, D. A., L. A. Toledo Machado, H. Laurent, and I. Velasco (2008), Forecast and Tracking the Evolution of Clouds Clusters (ForTraCC) using satellite infrared imaginary: Methodology and validation, *Weather Forecast.*, *23*, 233–245, doi:10.1175/2007WAF2006121.1.

Vila, D. A., L. G. de Goncalves, D. L. Toll, and J. R. Rozante (2009), Statistical evaluation of combined daily gauge observations and rainfall satellite estimates over continental South America, *J. Hydrometeorol.*, *10*, 533–543, doi:10.1175/2008JHM1048.1.

Wilson, C. B., J. B. Valdes, and I. Rodriguez-Iturbe (1979), On the influence of the spatial distribution of rainfall on storm runoff, *Water Resour. Res.*, *15*, 321–328, doi:10.1029/WR015i002p00321.

Xie, P., and P. A. Arkin (1995), An intercomparison of gauge observations and satellite estimates of monthly precipitation, *J. Appl. Meteorol.*, *34*, 1143–1160, doi:10.1175/1520-0450(1995)034<1143:AIOGOA>2.0.CO;2.

Younger, P. M., J. E. Freer, and K. J. Beven (2009), Detecting the effects of spatial variability of rainfall on hydrological modelling within an uncertainty analysis framework, *Hydrol. Processes*, *23*, 1988–2003, doi:10.1002/hyp.7341.

Zipser, E. J., C. Liu, D. J. Cecil, S. W. Nesbitt, and D. P. Yorty (2006), Where are the most intense thunderstorms on Earth?, *Bull. Am. Meteorol. Soc.*, *87*, 1057–1071, doi:10.1175/BAMS-87-8-1057.

E. M. C. Demaria and J. B. Valdes, Department of Hydrology and Water Resources, University of Arizona, 1133 E. James Rogers Way, Harshbarger Bldg. 11, Rm. 122, PO Box 210011, Tucson, AZ 85721-0011, USA. (edemaria@email.arizona.edu)

E. E. Ebert, Centre for Australian Weather and Climate Research, Melbourne, VIC 3001, Australia.

D. A. Rodriguez, Earth System Science Center, National Institute for Space Research, Cachoeira Paulista 12630-000, Brazil.

P. Salio, Centro de Investigaciones del Mar y la Atmósfera, CONICET/UBA, Universidad de Buenos Aires, Intendente Guiraldes 2160, Ciudad Universitaria Pabellón II-2do. Piso (C1428EGA), Buenos Aires, Argentina.

F. Su, Department of Civil and Environmental Engineering, University of Washington, Seattle, WA 98195, USA.